

Particle Physics Research Centre  
School of Physics and Astronomy  
Queen Mary University of London

## **Measurements of $H \rightarrow b\bar{b}$ decays and $VH$ production**

Thomas Charman

Supervisor: Dr. Jonathan Hays

Submitted in partial fulfillment of the requirements of the Degree of Doctor of  
Philosophy May 18, 2020.

I, Thomas Paul Charman, confirm that the research included within this thesis is my own work or that where it has been carried out in collaboration with, or supported by others, that this is duly acknowledged below and my contribution indicated. Previously published material is also acknowledged below.

I attest that I have exercised reasonable care to ensure that the work is original, and does not to the best of my knowledge break any UK law, infringe any third party's copyright or other Intellectual Property Right, or contain any confidential material.

I accept that the College has the right to use plagiarism detection software to check the electronic version of the thesis. I confirm that this thesis has not been previously submitted for the award of a degree by this or any other university.

The copyright of this thesis rests with the author and no quotation from it or information derived from it may be published without the prior written consent of the author.

Signature:

Date:

Details of collaboration and publications:

# Contents

<b>List of Figures</b>	<b>4</b>
<b>List of Tables</b>	<b>4</b>
<b>1 The ATLAS Detector at the Large Hadron Collider</b>	<b>5</b>
1.1 The Large Hadron Collider . . . . .	6
1.2 The ATLAS Detector . . . . .	8
Inner Detector . . . . .	11
Pixel Detectors . . . . .	12
Semiconductor Tracker . . . . .	13
Transition Radiation Tracker . . . . .	14
Calorimeters . . . . .	14
Electromagnetic Calorimeter . . . . .	15
Hadronic Calorimeter . . . . .	16
Muon Spectrometers . . . . .	16
Trigger Systems . . . . .	16

# List of Figures

1.1	Representation of an idealised set of coil magnets in a quadrupole configuration. Magnetic field lines are shown in black and forces acting on a bunch of protons, represented by a red ellipse, are shown in blue. . . . .	5
1.2	A representation of a dipole magnet, the magnetic field it generates and the force it imparts on a charged particle. . . . .	6
1.3	The CERN accelerator complex . . . . .	7
1.4	The ATLAS Detector . . . . .	9
1.5	ATLAS magnetic field . . . . .	11
1.6	ATLAS inner detector . . . . .	12
1.7	ATLAS long strip module . . . . .	13
1.8	ATLAS strip close-up . . . . .	14
1.9	ATLAS Calorimeter . . . . .	15
1.10	ATLAS muon subsystem . . . . .	17

# List of Tables

# Chapter 1

## The ATLAS Detector at the Large Hadron Collider

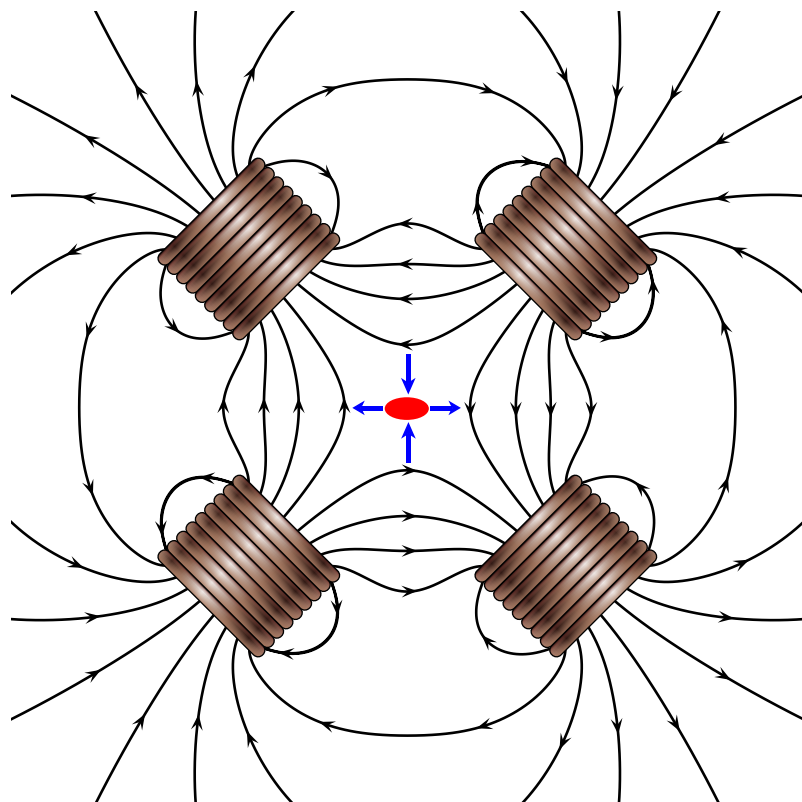


Figure 1.1: Representation of an idealised set of coil magnets in a quadrupole configuration. Magnetic field lines are shown in black and forces acting on a bunch of protons, represented by a red ellipse, are shown in blue.

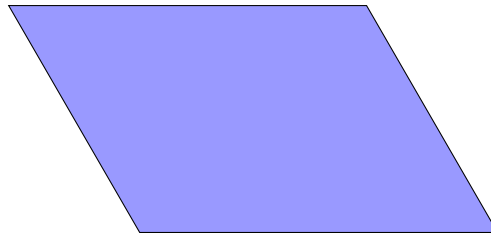


Figure 1.2: A representation of a dipole magnet, the magnetic field it generates and the force it imparts on a charged particle.

## 1.1 The Large Hadron Collider

The Large Hadron Collider (LHC) [1] is a large circular machine located 100 m underground straddling the Swiss-French border at the European Organisation for Nuclear Research (CERN). The machine is primarily a proton collider <sup>1</sup> and is designed so that protons may be accelerated over to very high energies before being allowed to collide. The diameter of the LHC is 27 km, it resides in a tunnel which was originally excavated for the Large Electron-Positron Collider [2] experiment and at the time was the largest civil engineering project in Europe. Today there are many experiments at CERN, all with the goal of improving our understanding of a particular area of physics some of which are marked in figure. 1.3. In particular there are seven experiments that record data from the collisions at the LHC: ATLAS [3], CMS [4], LHCb [5], ALICE [6], MoEDAL [7], TOTEM [8] and LHCf [9].

The LHC receives protons that have already been accelerated somewhat by the Super Proton Synchrotron (SPS), another of the accelerators at the CERN accelerator complex shown in figure 1.3. The circular design of both the LHC and SPS allows protons to be accelerated many times around their respective rings until their velocity is fast enough for a high energy collision. The highest energy collisions achieved take place at a centre of mass energy of  $\sqrt{s} = 13$  TeV, although the design energy of the LHC is  $\sqrt{s} = 14$  TeV. Despite having not yet reached its design energy the LHC collides particles with the highest energy of any particle collider in history and is currently alone at the energy frontier of modern physics. At the time of writing the LHC is in its second long shutdown during which maintenance and

---

<sup>1</sup>The LHC also collides other charged particles such as ions of lead or xenon.

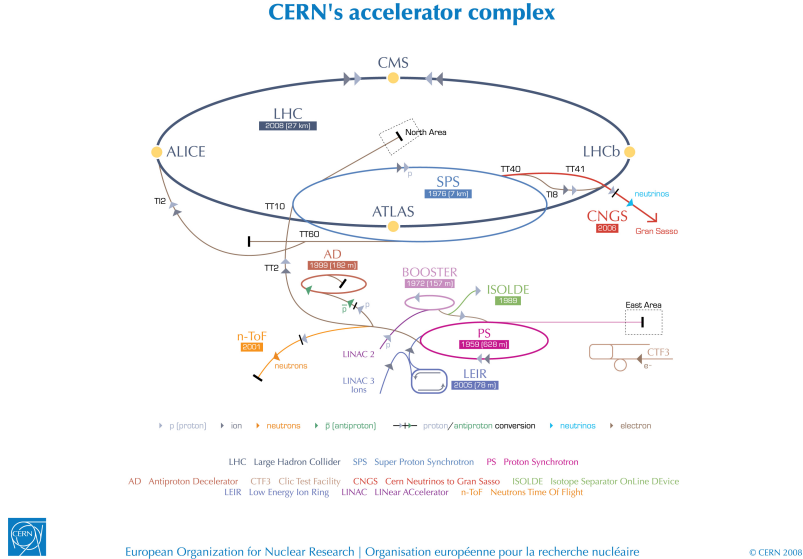


Figure 1.3: The CERN accelerator complex [10].

upgrades to the LHC and the particle detectors located around its ring take place. The LHC has completed two runs data taking from collisions, Run 1 took place from 2009 to 2013, followed by Run 2 between 2015 and 2018. The period between runs is known as long shutdown 1 (LS1), and was used to perform maintenance and upgrades. Many analyses from Run 1 have been published including, most notably the discovery of the Higgs boson [11, 12]. Some Run 2 analyses have also published results a highlight of which is LHCb’s discovery of charge parity violation in charm decays [13]. Despite these impactful results there are many more results expected from the LHC experiments as data continues to be analysed.

The statistical nature of particle physics analyses means that larger datasets (more recorded collisions) increase the sensitivity of searches and measurements. Constraints on the number of years the LHC is able to run mean that the best way to record more collisions is to collide more particles per second. A quantity known as the luminosity is often used to describe how much data is available for an analysis, it is written as

$$L = \frac{1}{\sigma} \frac{dN}{dt}, \quad (1.1)$$

where  $\sigma$  is the interaction cross-section, a volume within which particles must pass by one another in order to interact, and  $N$  is the number of events recorded in a

period of time  $t$ . For luminosity at the LHC  $N$  can be expressed as

$$N = n_{bp}n_1n_2\nu_r, \quad (1.2)$$

where  $n_{bp}$  is the number of colliding bunch pairs,  $n_1$  and  $n_2$  are the number of protons in each beam and  $\nu_r$  is the frequency with which the beams rotate around the LHC's circumference. It is clear that to increase luminosity any one of these parameters can be increased. The LHC has already exceeded it's design luminosity providing physicists with more data to analyse than expected and plans are well underway for the upgrade to a High-Luminosity LHC (HL-LHC) [14].

## 1.2 The ATLAS Detector

The ATLAS detector [15] resides at a location on the LHC ring called Point 1, its full name is A Toroidal LHC ApparatuS. A diagram of the detector is shown in figure 1.4. ATLAS is considered to be a general purpose particle detector and has a wide physics program including: Higgs boson physics, top quark physics, searches for Supersymmetry and exotic states, probes of CP violation in b-quarks and light states and heavy ion physics. The work in this report is concerned with the measurement of products from proton-proton collisions. The detector itself is very large in size, spanning a width of 25 m and a length of 44 m and weighs 7000 tonnes which is comparable to the weight of the wrought iron content of the Eiffel tower [16].

Due to the composite nature of the proton, the decay products of collisions are extremely numerous. Additionally when two bunches of protons cross there is the chance that more than one hard scattering event occurs and softer glancing collisions are also a possibility. The number of hard scattering events in a given bunch crossing is known as the pile-up of the collision and is often denoted with the symbol  $\mu$ . As can be seen by inspecting equations 1.2 and 1.1 increasing the luminosity will often cause a higher pile-up environment in the detector. High pile-up, along with

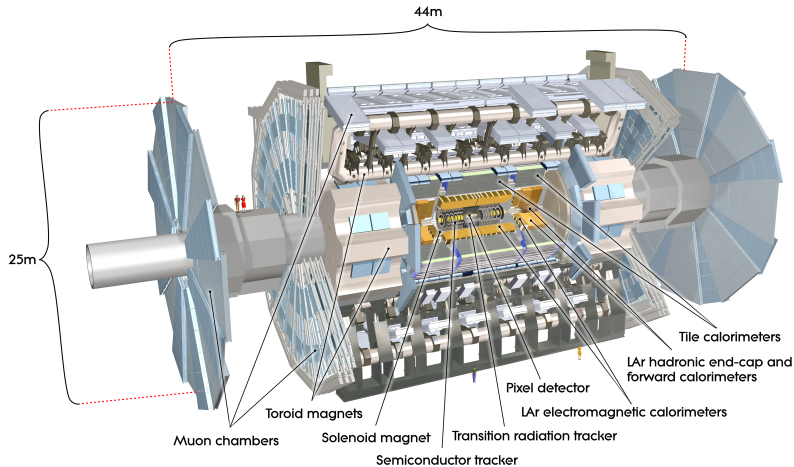


Figure 1.4: Computer generated image of the whole ATLAS detector with the major sub detectors labeled [17].

the numerous decay products of each collision necessitate the use of specialised sub-detectors in order to accurately measure the output of collisions. For certain types of decay product there are different dedicated sub-systems in ATLAS with the purpose of measuring properties of particles of that type. At this stage it is sufficient to say that the treatment of electrically charged particles must be different to those that are electrically neutral, but this concept will be expanded upon in more detail in the further sections. It is interesting to note that despite the many charges that are associated with the forces of nature discussed in chapter ?? the only one that we can directly measure is electric charge.

The ATLAS sub-systems are located in either the barrel of the detector or one of the end-caps. These two areas have a different geometry and so the design of a sub-system in the barrel will differ from the same sub-system in the end-cap. What follows is a description of the ATLAS sub-systems and their individual components, for each component more detail will be given about which properties of which types of particles it is used to measure. These details are based on the ATLAS technical design report volumes [18, 19] unless another citation is present. Before detailing individual components it is important to detail certain properties of the detector relevant to all sub-systems. The coordinate system used to describe the ATLAS detector is known as right-handed. Three orthogonal axes ( $x, y, z$ ) are used to

describe the 3D space of the detector. The x-axis points towards the centre of the LHC ring, the y-axis points upwards and the z-axis points along the LHC beam pipe y-axis. The three axes meet at the interaction point which is the nominal position where bunches cross, located in the centre of the detector. Cylindrical coordinates  $(r, \phi)$  are also often used to describe the physical features of the detector and phenomena caused by interactions in the detector that shall be referred to as analysis objects. Their definitions are that  $\phi$  is the azimuthal angle in the x-y plane (transverse) around the beam pipe and  $r$  is the distance from the interaction point. A final quantity used due to its compatibility with description relativistic objects in the detector is pseudo-rapidity  $\eta = -\ln(\tan(\theta/2))$  where  $\theta$  is the zenith angle measured from the z-axis.

The grouping of particles into electrically charged or neutral is largely due to the fact charged particles experience the Lorentz force

$$\vec{F} = q(\vec{E} + \vec{v} \times \vec{B}), \quad (1.3)$$

whereas neutral particles have  $q = 0$ , and so they do not. The magnetic field  $\vec{B}$  has the effect of changing the direction of the particles trajectory only. This is due to the fact that any force  $\vec{F}$  resulting from the cross product of two vectors, in this case the field vector and the velocity  $\vec{v}$ , must act in a perpendicular to the two crossed vectors and thus perpendicular to the direction of the motion (the direction of velocity). Similarly the electric field term  $\vec{E}$  has the effect that the particle is accelerated in the direction (or opposite in the case of a negative particle) of the field lines. The consequence of this is that in a known magnetic field the velocity of a particle can be calculated by measuring the radius of curvature of its trajectory. In order to exploit these properties of charged particles a large portion of the ATLAS detector is immersed in magnetic fields created by the magnet systems. There are four magnet systems in ATLAS the solenoid, the barrel toroid, and two end-cap toroids. The solenoid surrounds the inner detector whilst the toroid systems surround the muon chambers. Figure 1.5 shows a heat map of the magnetic field

strengths within ATLAS, the image is from an article detailing the superconducting magnet system [20]. The magnet systems store a total energy of 1.6 GJ and produce fields of a combined volume of approximately  $12 \times 10^4 \text{ m}^3$ .

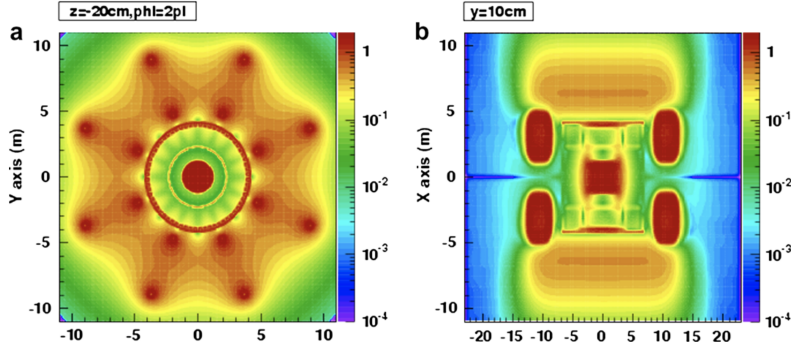


Figure 1.5: ATLAS magnetic field profile, showing a transverse cross-section in the centre of the detector (a), and a longitudinal section (b) [20].

## Inner Detector

The Inner Detector (ID) is comprised of pixel detectors, the semiconductor tracker (SCT) and a transition radiation tracker (TRT) as seen in figure 1.6. It covers a volume corresponding with the total  $\phi$  angle. In relation to  $\eta$  the pixel detectors and SCT cover the range  $|\eta| < 2.5$  and the TRT covers  $|\eta| < 2.0$ . Being the innermost sub-detector of ATLAS the primary goals of the ID are to reconstruct the locations of the origin of interactions (known as the interaction vertex), and to track the propagation of charged particles through the detector. This is achieved by measuring a sequence of hits for each charged particle that propagates through its material, upon which reconstruction algorithms can be applied, known as track finding algorithms. From this sequence of hits interaction vertices can also be reconstructed, the vertex which comes from the highest energy collision in a given event is known as the primary vertex. Information from the tracker is used to match activity in outer regions of the detector to an interaction vertex. Each reconstructed track will have a momentum assigned to it, which is calculated using equation 1.3. The magnetic field that the ID is immersed in is produced by the solenoid magnet

system. The system is made of a single layer coil with an inner diameter of 2.46 m and produces 2 T field in the axial direction with respect to the beam-pipe.

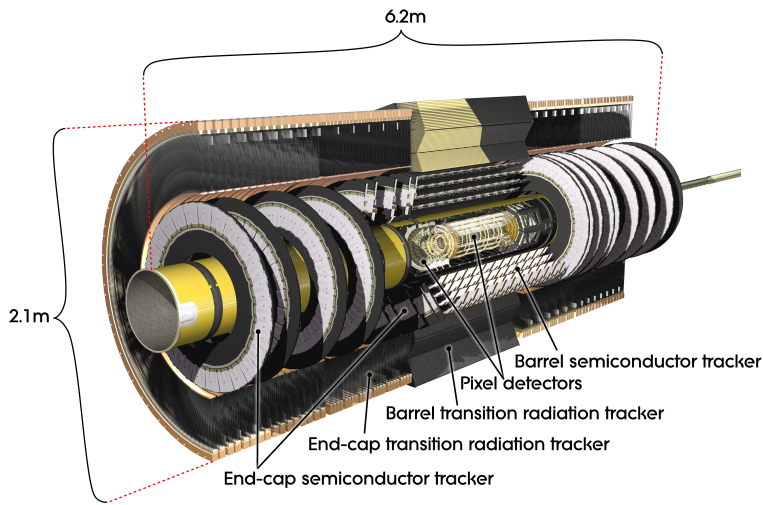


Figure 1.6: Computer generated image of the ATLAS inner detector [21].

## Pixel Detectors

There are four layers of pixel detectors that are the closest components of the ID to the beam-pipe. The design originally had three layers, each 250  $\mu\text{m}$  thick with 50  $\mu\text{m}$  by 250  $\mu\text{m}$  pixels, of oxygen doped n-type silicon crystals. During LS1 a fourth layer, closest to the beam-pipe (which was also replaced for a smaller radius version) was added. This layer is known as the insertable B-layer (IBL) [22], the motivation for its addition was to counteract degradation of original performance of the ID due to irreversible damage by radiation. As well as the inclusion of the IBL, performance degradation is mitigated by increasing the bias voltage across the pixels from 100 V (their starting voltage) to up to 600 V. Additionally the IBL being closer to the beam-pipe allows for interaction vertices to be measured more precisely. The need for better reconstruction of vertices is motivated by their role in the performance of algorithms that classify jets of activity in the detector that are initiated by B-hadrons, this is where the IBL gets its name. There are no pixel detectors in the end-caps.

## Semiconductor Tracker

Next closest to the beam-pipe are the semiconductor trackers. Similarly to the pixel detectors the semiconductor trackers are also made of silicon. In contrast to the n-type silicon of the pixels, the semiconductor trackers use p-in-n type technology. The semiconductor modules are comprised of two back to back silicon wafers that are offset by a small angle in order to improve coverage. Each wafer has a series of strips of p-in-type material covered in a metalised layer, the strips are separated by a distance of  $80 \mu\text{m}$ . The strips have a bias voltage applied and on the wafers the necessary electronics are mounted for readout as seen in figure 1.7. In order

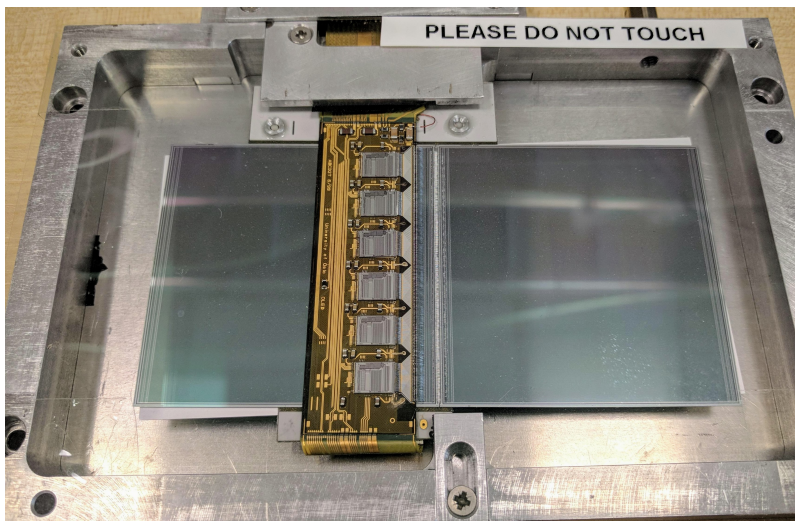


Figure 1.7: An image of an SCT long strip module mounted in a rig for testing at Queen Mary University of London.

to calibrate the response of the strips a  $100 \text{ M}\Omega$  poly-silicon resistor is located at the end of each strip. Figure 1.8 shows an image of the snake-like structure of a poly-silicon resistor from the end of an SCT module. The modules come in two different designs, short strips and long strips with the short strips forming the layer closest to the pixel detectors and the long strips on the outside.

The original operating bias voltage was 150 V but again due to radiation exposure this will raise to up to 350 V over time as necessary. There are four layers of semiconductor trackers in the barrel arranged so that sensors have a tilt with respect to a perfect coaxial cylinders of approximately  $11^\circ$ . This tilt increases the amount

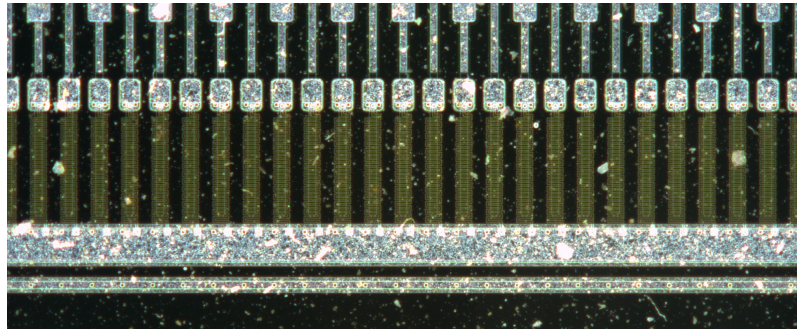


Figure 1.8: A close up image of the end of an SCT sensor in which the snake-like poly-silicon resistors are visible as a yellowish coloured structure at the end of each strip. This image was taken with a high resolution automatic area scanner commissioned by the author [23] in order to take full scans of strip sensors during the production of the ATLAS Inner Detector upgrade known as the Inner Tracker (ITk) [24, 25].

of material that particles will travel through and is optimized to the geometry of the detector. Similarly the end-cap modules are arranged in petal like structures, with a number of different geometric designed based on the position within the end-cap.

### Transition Radiation Tracker

The final layer of the ID is the TRT, the primary role of the TRT is to aid electron identification by measurement of transition radiation. The TRT is mostly made up of polyimide drift tubes with a diameter of 4 mm. The drift tubes are filled with a gas mixture whose majority constituent is xenon. These tubes operate with a voltage of -1530 V and are contained within a carbon fibre support structure. The geometrics layout of the tubes is optimized for both the barrel and end-caps.

### Calorimeters

The purpose of the calorimeters is to measure the total energy of particles that pass all the way through the ID, this is achievable only if the calorimeter stops the particle completely. A desirable side effect is that they also act as a barrier to stop particles passing through to the muon spectrometers, of course this means necessarily that muons pass through the calorimeters. There are two calorimeter systems in ATLAS the electromagnetic calorimeter (ECAL) and the hadronic calorimeter (HCAL), they

will be explained in the following sections. The calorimeters are not immersed in a significant magnetic field compared to the rest of the ATLAS as seen in the heat map of figure 1.5. This is because measuring the energy of

particles and acting as a barrier to them does not require curved trajectories.

The geometric layout of the calorimeter systems, as well as the location of specific components can be seen in figure 1.9, in which the ID can also be seen (greyed out). Information from the two calorimeters is used in conjunction for any particles whose decay products propagate through both volumes. Both calorimeters are split up into cells of material that are used to determine the position of decay products in the detector.

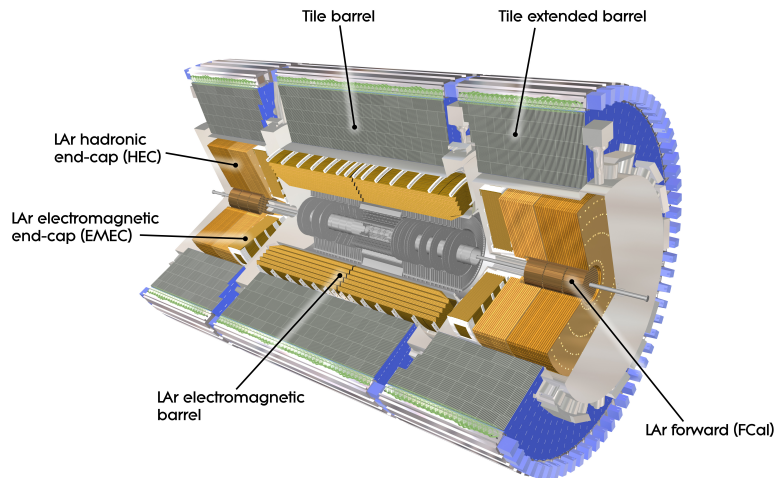


Figure 1.9: Computer Generated image of the ATLAS calorimeter [26].

### Electromagnetic Calorimeter

The ECAL is primarily concerned with measuring the energy and stopping the trajectory of electrons and photons. It has liquid argon (LAr) as it's active material. Particles initiate an electromagnetic shower of decay products in the active material which ionizes it. An applied electric field causes these ions to drift in such a way that the current induced is proportional to the energy deposited by the incident particle.

## Hadronic Calorimeter

The HCAL also has a LAr component which works in a similar way to that of the ECAL but with different optimizations for the HCAL's specialised design. The HCAL is specifically tasked with measuring the energy and stopping the trajectory of hadrons. The HCAL also contains a tile calorimeter which uses scintillation light produced in the tiles as a means to measure the deposited energy of hadrons.

## Muon Spectrometers

Surrounding the calorimeters are the muon spectrometers, which form the most outer layer of the detector. Though muons are charged leptons just like electrons, their specific properties mean that dedicated muon spectrometers are required to detect them. Muons deposit far less energy per distance traveled than other particles meaning that they punch through most materials with ease. As can be seen in figure 1.10 the components of the muon spectrometers are the thin-gap chambers, cathode strip chambers, resistive plate chambers and monitor drift tubes. The barrel and end-cap toroid magnets immerse the muon spectrometers in a magnetic field which at its peak (visible in figure 1.5) has a strength of 4 T. Despite a stronger peaking magnetic field than in the solenoid observed muon tracks are often far less curved than that of their lighter cousins, the electrons. This is due to the larger mass of the muon. Muons do leave tracks in the ID and also deposit small amounts of energy in the calorimeters. Tracks in the muon spectrometers are matched up to tracks in the ID with the aid of the location of energy deposits in the calorimeters if possible. The full tracking information for muons can be used in algorithms such as overlap removal, which is used to remove muons from jets that they have been erroneously associated with by matching the muon with its ID track.

## Trigger Systems

The trigger systems in ATLAS allows data to be recorded only when an event meets certain criteria. Without triggering there would be no way to decide which events

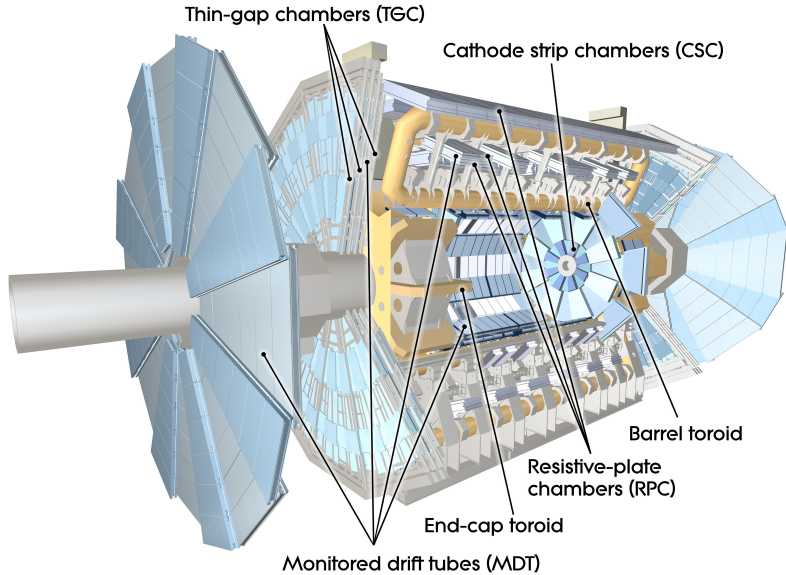


Figure 1.10: Computer generated image of the ATLAS Muons subsystem [27].

to readout and which to ignore. It would be impossible to readout every interaction that occurs in the detector. The reason for this is that the geometric constraints of the detector mean that there is only a small space available for readout wires, as detection medium needs to be prioritized for sensitivity and technology limits the data rate that one can achieve through a cable of fixed area. The trigger system comes in two parts, a hardware component referred to as level one (L1) and software component referred to as the high level trigger (HLT). The L1 system is comprised of the L1 calorimeter (L1Calo) trigger which operates by searching for clusters of energy in the calorimeters and the L1 muon (L1Muon) system which coincidences in the muon systems. A third system L1 topological (L1Topo) uses regions of interest built from the L1Calo and L1Muon data which are passed to central trigger processors for selection. The various limitations of the hardware mean that these selections must be passed up to the next level of triggering, the HLT in a time window of  $2.5 \mu\text{s}$ . The HLT takes information from the L1 systems and uses faster versions of an offline style analysis in order to select or reject events for readout. In order for a trigger to fire an event must pass fully all of the requirements of one of the algorithms defined by an extensive trigger menu. More information about the triggers used in the  $VH(bb)$  analysis will be given in a later chapter.

# Bibliography

- [1] Oliver Sim Brüning, Paul Collier, P Lebrun, Stephen Myers, Ranko Ostojic, John Poole, and Paul Proudlock. *LHC Design Report*. CERN Yellow Reports: Monographs. CERN, Geneva, 2004. URL <https://cds.cern.ch/record/782076>.
- [2] *LEP design report*. CERN, Geneva, 1984. URL <https://cds.cern.ch/record/102083>. Copies shelved as reports in LEP, PS and SPS libraries.
- [3] CERN. ATLAS: Letter of intent for a general purpose p p experiment at the large hadron collider at CERN. 1992.
- [4] M. Della Negra et al. CMS: letter of intent by the CMS Collaboration for a general purpose detector at LHC. Technical Report CERN-LHCC-92-003. LHCC-I-1, CERN, Geneva, 1992. URL <https://cds.cern.ch/record/290808>. Open presentation to the LHCC 5 November 1992, M. Della Negra/CERN, CMS Spokesman.
- [5] H. Dijkstra, Hans Jürgen Hilke, Tatsuya Nakada, and Thomas Ypsilantis. LHCb Letter of Intent, LHCb Collaboration. 1995.
- [6] Letter of Intent for A Large Ion Collider Experiment [ALICE]. Technical Report CERN-LHCC-93-016. LHCC-I-4, CERN, Geneva, 1993. URL <https://cds.cern.ch/record/290825>.
- [7] G Giacomelli, A A Faust, and James L Pinfold. A search for highly ionizing particles and slow exotic decays at the LHC using the MOEDAL detectors:

- letter of intent. Technical Report CERN-LHCC-98-05. LHCC-I-19, CERN, Geneva, Feb 1998. URL <https://cds.cern.ch/record/347906>.
- [8] W Kienzle, , et al. *Total cross section: elastic scattering and diffraction dissociation at the LHC.* Letter of Intent. CERN, Geneva, 1997. URL <http://cds.cern.ch/record/335255>.
- [9] O Adriani. LHCf Letter of Intent for a p-Pb run. A precise study of forward physics in  $\sqrt{s_{NN}} = 4.4$  TeV proton-Lead ion collisions with LHCf at the LHC. Technical Report CERN-LHCC-2011-015. LHCC-I-021, CERN, Geneva, Dec 2011. URL <https://cds.cern.ch/record/1404163>.
- [10] Christiane Lefèvre. The CERN accelerator complex. Complexe des accélérateurs du CERN. Dec 2008. URL <https://cds.cern.ch/record/1260465>.
- [11] Georges Aad et al. (ATLAS Collaboration). Observation of a new particle in the search for the Standard Model Higgs boson with the ATLAS detector at the LHC. *Phys. Lett.*, B716:1–29, 2012. doi: 10.1016/j.physletb.2012.08.020.
- [12] Serguei Chatrchyan et al. (CMS Collaboration). Observation of a new boson at a mass of 125 GeV with the CMS experiment at the LHC. *Phys. Lett.*, B716: 30–61, 2012. doi: 10.1016/j.physletb.2012.08.021.
- [13] Roel Aaij et al. Observation of CP Violation in Charm Decays. *Phys. Rev. Lett.*, 122(21):211803, 2019. doi: 10.1103/PhysRevLett.122.211803.
- [14] I. Bejar Alonso and L. Rossi. HiLumi LHC Technical Design Report. 2015.
- [15] Georges Aad et al. (ATLAS Collaboration). The atlas experiment at the cern large hadron collider. *Journal of Instrumentation*, 3(08):S08003, 2008. URL <http://stacks.iop.org/1748-0221/3/i=08/a=S08003>.
- [16] David Hanser. *Architecture of France*. Greenwood Press, Westport, Conn, 2006. ISBN 978-0-313-31902-0.

- [17] Joao Pequenao. Computer generated image of the whole ATLAS detector. Mar 2008. URL <https://cds.cern.ch/record/1095924>.
- [18] A. Airapetian et al. ATLAS: Detector and physics performance technical design report. Volume 1. 1999.
- [19] A. Airapetian et al. ATLAS: Detector and physics performance technical design report. Volume 2. 1999.
- [20] H.H.J. ten Kate. The atlas superconducting magnet system at the large hadron collider. *Physica C: Superconductivity*, 468(15):2137 – 2142, 2008. ISSN 0921-4534. doi: <https://doi.org/10.1016/j.physc.2008.05.146>. URL <http://www.sciencedirect.com/science/article/pii/S0921453408004541>. Proceedings of the 20th International Symposium on Superconductivity (ISS 2007).
- [21] Joao Pequenao. Computer generated image of the ATLAS inner detector. Mar 2008. URL <https://cds.cern.ch/record/1095926>.
- [22] M Capeans, G Darbo, K Einsweiller, M Elsing, T Flick, M Garcia-Sciveres, C Gemme, H Pernegger, O Rohne, and R Vuillermet. ATLAS Insertable B-Layer Technical Design Report. Technical Report CERN-LHCC-2010-013. ATLAS-TDR-19, Sep 2010. URL <https://cds.cern.ch/record/1291633>.
- [23] Thomas Paul Charman, Bart Hommels, and Adrian John Bevan. Authorship Qualification Task: ATLAS ITk Sensor Scanner Documentation (QMUL). Technical Report ATL-COM-ITK-2019-018, CERN, Geneva, Jan 2019. URL <https://cds.cern.ch/record/2674404>.
- [24] Ben Brueers. The design and layout of the Phase-II upgrade of the Inner tracker of the ATLAS experiment. Jul 2019. URL <https://cds.cern.ch/record/2681301>.
- [25] John Stakely Keller. The ATLAS ITk Strip Detector System for the Phase-II LHC Upgrade. Feb 2019. URL <https://cds.cern.ch/record/2663172>.

- [26] Joao Pequenao. Computer Generated image of the ATLAS calorimeter. Mar 2008. URL <https://cds.cern.ch/record/1095927>.
- [27] Joao Pequenao. Computer generated image of the ATLAS Muons subsystem. Mar 2008. URL <https://cds.cern.ch/record/1095929>.